WWJMRD 2026; 12(05): 06-12
www.wwjmrd.com
International Journal
Peer Reviewed Journal
Refereed Journal
Indexed Journal
Impact Factor SJIF 2017: 5.182 2018: 5.51, (ISI) 2020-2021: 1.361
E-ISSN: 2454-6615

Alfred Rufer
Ecole Polytechnique Fédérale de Lausanne, STI-DO, CH1015 Lausanne, Switzerland.

Correspondence:
Alfred Rufer
Ecole Polytechnique Fédérale de Lausanne, STI-DO, CH1015 Lausanne, Switzerland.

A New Compressed Air Engine based on Pneumatic Artificial Muscles (PAMs)

Alfred Rufer

Abstract
A compressed air engine based on pneumatic artificial muscles is analysed and modelled. Pneumatic artificial muscles (PAMs) offer several advantages over conventional pneumatic cylinders: a high force-to-weight ratio, a flexible structure, minimal compressed air consumption, availability in various sizes, low cost, and high reliability. From a kinematic model of the complete mechanism, the simulation calculates instantaneous system variables such as forces, torque, and power. Energetic properties in terms of efficiency are also evaluated. The study is completed by the realisation of an experimental set-up that validates a key design innovation. The presented results explain in detail the operating principle and describe the behavior through simulation. Additionally, an original sliding anchor element, developed to resolve an inherent kinematic problem of such motors, is introduced and its function verified.

Keywords: compressed air engine; pneumatics; artificial muscle; simulation; energy efficiency.

Introduction
Compressed air engines have been proposed in many contexts of use and across many different technologies. Their primary advantages include technological simplicity, high reliability, and low acquisition costs [1]. Beyond standard industrial applications in production, handling, or automation, a significant application field is the energy sector. Specifically, they are used in compressed air energy storage (CAES) systems as conversion engines in the recovery path between the storage vessel and the electrical generator [1]. The classical compressed air machines range from rotary vane to piston/crankshaft types, through gear or turbine-type motors. In general, these motors exhibit low energetic efficiency due to their conversion principle, where only displacement work is produced in the machine [2–4]. Recent developments in pneumatic-to-mechanical conversion, however, have enabled a significant increase in the energetic performance of such machines. These benefits are realized by adding a second torque component to the conversion principle, resulting from a true thermodynamic expansion inside the active volume or in a supplementary, larger chamber [5–7].
Pneumatic drives for vehicle propulsion have also been proposed, demonstrating widely varying energetic performances. These have included transformed internal combustion engines for zero-emission vehicle applications as well as dedicated architectures designed for increased efficiency [8–12].
A novel approach for the realization of compressed air engines, first presented in [13], utilizes pneumatic artificial muscles (PAMs) as the primary actuators. As illustrated in the assembly diagram shown in Figure 1, this engine concept utilizes two PAMs acting in opposition on a central crankshaft. Pneumatic artificial muscles offer several advantages over conventional pneumatic cylinders, including a superior force-to-weight ratio, a flexible structure, minimal compressed air consumption, availability in various sizes, low cost, and high reliability. The low compressed air consumption is a direct result of the PAM's small internal volume; its high force-to-weight ratio allows it to generate significant traction forces with minimal air mass, a characteristic well-documented in the literature [14–18].

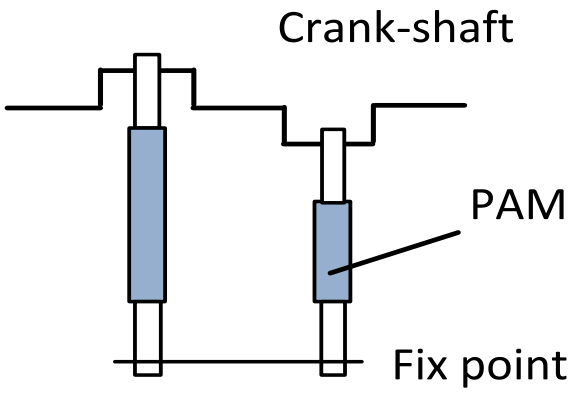

Fig. 1: System assembly

The purpose of the present paper is to comprehensively model and investigate the PAM-based compressed air motor concept from [13], establishing a formal methodology for representing its behavior and evaluating its performance. To achieve this, it is first necessary to accurately characterize the force-generating properties of the PAMs themselves. The resulting component model is then integrated into a full kinematic simulation of the engine to calculate force, torque, and other key variables. From this, the energetic properties of the engine are evaluated. A primary objective is to verify the potential of this type of pneumatic actuator for use in the energy recovery path of CAES systems. The contribution first analyzes the kinematics of the system assembly, which consists of a crankshaft and a variable-length active connecting rod. As shown in the conceptual overview (Fig. 1), the studied system features a crankshaft with two connecting rods operating in alternation. In the global model, the forces exerted on the pins of the crankshaft are derived from the non-linear force-elongation function of the PAM. Subsequently, the produced torque and mechanical power are calculated. Using these quantities and considering the enthalpy of the injected air, the energetic efficiency of the engine is evaluated. This theoretical study and simulation are then complemented by an experimental set-up used for practical verification of key design elements.

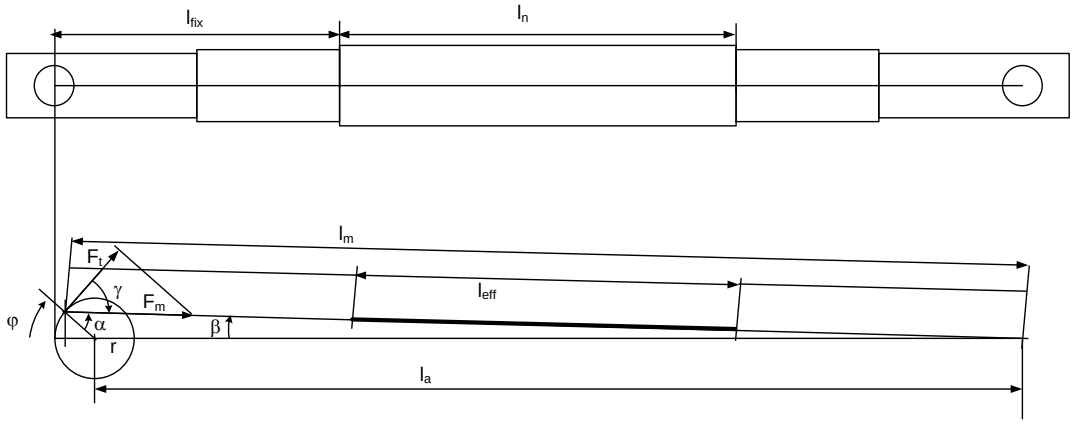

Fig. 2 Geometry of the assembly with parameters

2. Kinematic model of the engine

Figure 2 shows, at the top, the complete active connecting rod, composed of the PAM itself flanked by coupling elements in the form of joint head bearings. In the lower portion of the figure, the system assembly is represented with the crankpin's circular trajectory, the coupled active rod, and the key geometric parameters. These parameters, particularly the dimensions of the artificial muscle and its mechanical couplings, are critical for the model. The radius of gyration of the crankpins, r, is indicated. The value of r is selected to impose a variation of 20% of the PAM's nominal length. The length l_m of the complete active connecting rod, for a crankshaft rotation angle φ, is the sum of the effective PAM length l_{eff} and twice the length of the coupling elements l_{fix}. In the non-contracted state of the PAM, l_m takes the value l_{m0}:

$$l_{m0} = l_n + 2 \cdot l_{fix} = l_a + r$$

where l_n is the nominal length of the active part of the PAM and l_a is the distance between the crankshaft axis and the anchor point of the active connecting rod.

From the geometric definitions provided in Fig. 2, the variable length of the complete active rod, l_m, can be calculated as:

$$l_m = \sqrt{(l_a + r\cos\varphi)^2 + (r\sin\varphi)^2} \quad (1)$$

with

$$l_a = l_n + 2l_2 + 2l_{rot} - r \quad (2)$$

The angle φ is the angle of rotation of the crankshaft. The angles α and β, also defined, are used for the calculation of the tangential force and are given by:

$$\alpha = 180 - (180 - \varphi) - \beta = \varphi - \beta \quad (3)$$

$$\beta = \arcsin\frac{r\sin\varphi}{l_m} \quad (4)$$

The effective length of the PAM is therefore:

$$l_{eff} = l_m - 2l_2 - 2l_{rot} \quad (5)$$

and the force exerted on the crankpin is:

$$F_m = f(l_{eff}) \quad (6)$$

Here, $f(l_{eff})$ represents the characteristic force produced by the PAM, which is a non-linear function dependent on both the muscle's length and its internal pressure. As shown graphically by the manufacturer's data in Fig. 3, not only does the force vary with length, but the unloaded length itself (where zero force is produced) changes with supply pressure.

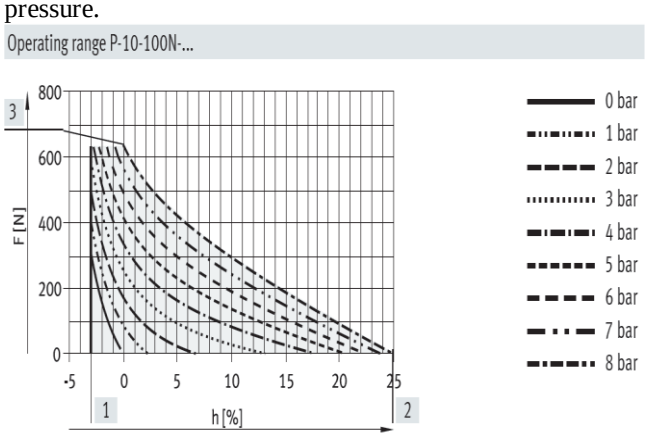

Fig. 3: Characteristic force produced by the PAM (adapted from typical manufacturer data).

This pressure-dependent free length creates a significant kinematic incompatibility with a fixed-radius crankshaft, a core challenge that must be addressed and that motivates the development of the sliding anchor mechanism discussed later in this paper.

Then, the tangential force on the crankshaft, F_t, becomes:

$$F_t = F_m \cdot \cos(\pi/2 - \alpha) \tag{7}$$

$$F_t = F_m \cdot \cos(\pi/2 - \varphi + arc\sin\frac{r\sin\varphi}{l_m}) \tag{8}$$

And the resulting torque, M, is:

$$M = F_t \cdot r \tag{9}$$

3. Simulation of the system

Based on relation (1) and the system parameter definitions in Fig. 2, the length of the complete active rod is calculated. Relations (3) and (4) are used for the two system angles, α and β. Subsequently, the effective length of the artificial muscle is determined using relation (5). The lengths of the two artificial muscles, which operate with a 180° phase-shift, are represented in Fig. 4.

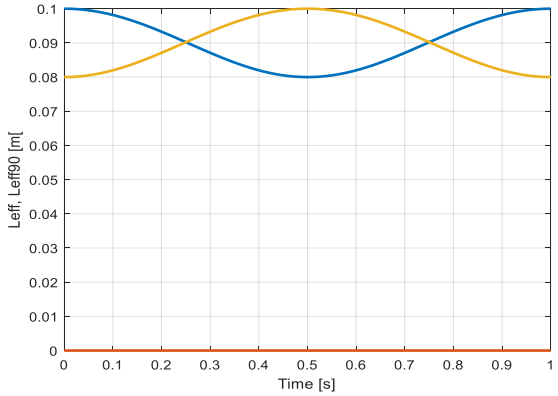

Fig. 4: Effective lengths of the artificial muscles

The simulation is performed at an angular velocity of 6.28 rad/s, corresponding to a rotation period of 1 second. As depicted in the plot, the effective lengths of the PAMs vary cyclically between 0.1 m and 0.08 m.

As described by relation (6), the force exerted on the crankpins is a function of the muscle's effective length. To ensure the simulation accurately reflected the behavior of the specific components used in the experimental setup, the empirical data from the manufacturer for a 4 bar pressure level was modeled using a mathematical function. By approximating the manufacturer's empirical data, a continuous function is derived that is essential for calculating the force at any intermediate length, thereby enabling a precise, step-by-step calculation of the tangential force and resulting torque throughout the crankshaft's rotation. The used approximation function is represented in Fig. 5

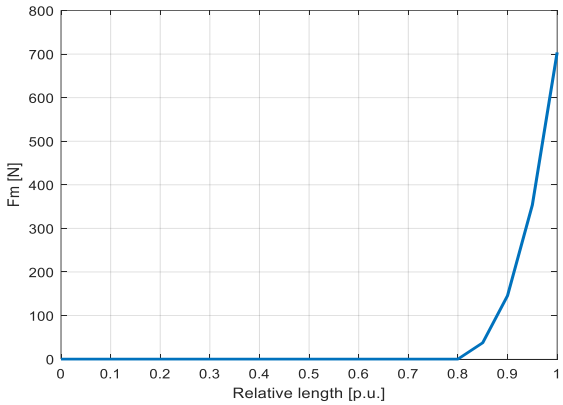

Fig. 5 Approximated form of the function for the force exerted by the muscle.

The force F_m exerted on the crankpins is parallel to the axis of the active connected rod which comprises the PAM. For the calculation of the torque developed by the engine, this force must be projected on a tangential axis according to relations (8). The curve obtained in the simulation for the tangential force F_t is represented in Figure 6. This figure represents the two forces exerted by the two PAM, namely a first contribution in the first half period and a second one in the second half period.

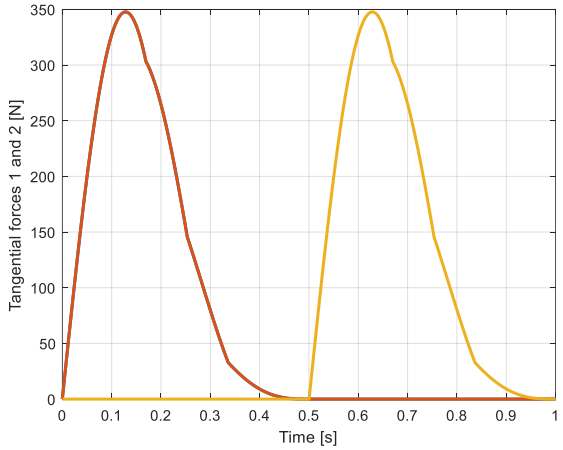

Fig. 6 Tangential force F_t developed by the engine (blue: first PAM, yellow: second PAM)

Finally, the total torque is calculated by the product of the tangential forces by the radius of gyration of the crankpins. The total torque is represented in Figure 7.

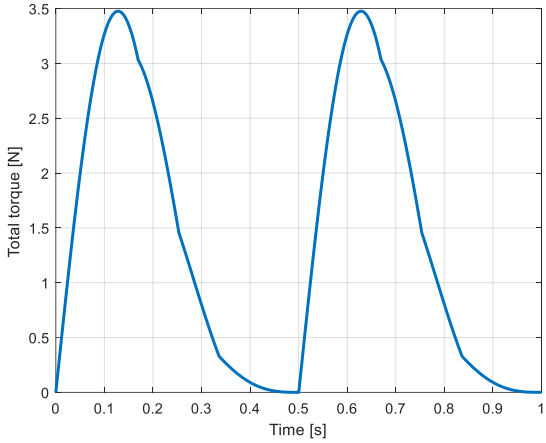

Fig. 7 Total torque developed by the engine.

The mechanical power is calculated as

$$P_{mech} = M \cdot \omega \qquad (10)$$

and is represented in Figure 8.

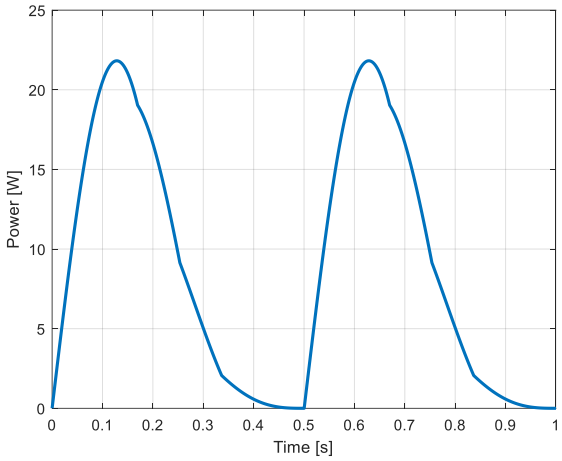

Fig. 8 Mechanical power

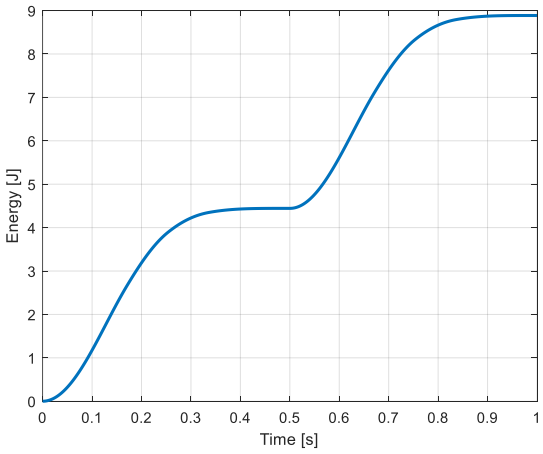

Fig. 9 Mechanical work produced by the engine

The simulation results presented here illustrate the operating principle of an air-driven motor based on the use of artificial muscles. The simulation has intentionally neglected some aspects of a real application as the mechanical friction of the crankshaft/connecting rod assembly which can strongly penalize the realization of such a system in a low power range. Another unknown is the power dissipation by the deformation of the flexible active part of the muscle. The relation between the diametral dilatation of the muscle and its axial contraction is guided by the stiff twine braids but include an elastic deformation of the rubber coat. In this part, some deformation energy is absorbed but a non-negligible part of it is returned in the recovery action. This means that the simulation gives information on an idealized behaviour, as also to be found in the following section dedicated to energetic efficiency. The results thus validate a concept from the point of view of its limitations in an idealized functioning, which already represents a basic evaluation for estimating the viability of the basic concept.

4. Efficiency of the engine

As mentioned in the introduction to this article, manufacturers of pneumatic artificial muscles (PAMs) claim that their devices generate significant tractive forces with minimal compressed air consumption. Therefore, the energy efficiency of PAM based engines is expected to be high. In reality the actual efficiency is considerably lower, as demonstrated in this section. To evaluate the energy efficiency of an engine, the ratio of the mechanical work produced, W_{out}, to the enthalpy, H_{in}, of the injected air is calculated (Equation 11).

$$\eta_{conv} = \frac{W_{out}}{H_{in}} = \frac{W_{out}}{U + P_{in} \cdot \Delta V} \qquad (11)$$

The value of the produced mechanical work W_{out} is obtained from the integration of the instantaneous power P_{mech} over one period of the motor-cycle:

$$W_{out} = \int_0^t P_{mech}(t)dt \qquad (12)$$

where P_{mech} is the product of the torque multiplied by the angular velocity

From the simulation results given in Figure 9 the numerical value of $W_{out} = 8.887\,J$ is obtained.

For the evaluation of the enthalpy injected into the PAMs, their volume in the pressurized state must be evaluated. Figure 10 gives the dimensions of the PAM under relaxed (a) and contracted (b) conditions.

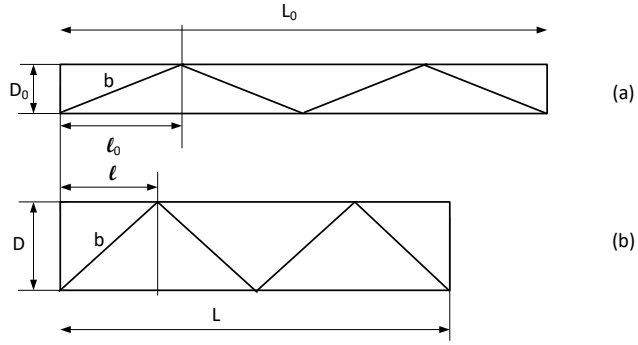

Fig. 10 Dimensions of the PAM

a) Relaxed state, b) Contracted state

The volume of the pressurized PAM is given by

$$V = \frac{\pi D^2}{4} L \tag{13}$$

where L and D are the length and the diameter of the PAM in its pressurized state

The diameter D is calculated with the assumption that the fiber-length of the mesh are of constant length (parameter b in Figure 10).

From the drawing of the relaxed state (Figure 10a), and if there are 4 "half-turns" of the twine braids over the length of the muscle, b is calculated as

$$b = \sqrt{l_0^2 + D_0^2} = \sqrt{(L_0/4)^2 + D_0^2} \tag{14}$$

and the diameter D of the contracted (pressurized) PAM is

$$D = \sqrt{b^2 - l^2} = \sqrt{b^2 - (L/4)^2} \tag{15}$$

The internal energy of the volume becomes

$$U = E_{comp} = P_{in} \cdot V_1 \left(\ln \frac{P_{in}}{P_{atm}} - 1 + \frac{P_{atm}}{P_{in}} \right) \tag{16}$$

Numerically, and considering the complete cycle (φ=0…2π) during which two fillings of the PAM's occur with air at 4 bar, U becomes

$$U = E_{comp} =$$

$$= 4 \cdot 10^5 N/m^2 \cdot 40.7 \cdot 10^{-6} m^3 \left(\ln \frac{4bar}{1bar} - 1 + \frac{1bar}{4bar} \right) =$$

$$= 10.36J \tag{17}$$

and

$$P_{in} \cdot \Delta V = 4 \cdot 10^5 N/m^2 \cdot 40.7 \cdot 10^{-6} m^3 = 16.28J \tag{18}$$

Finally the energetic efficiency becomes

$$\eta_{conv} = \frac{W_{out}}{H_{in}} = \frac{8.87J}{10.36J + 16.28J} = 0.332 \tag{19}$$

5. Experimental set-up

Figure 11 shows the experimental set-up with the crankshaft and the position sensor, the artificial muscles, the control valves and control circuits. At the left side of the figure 11a the sliding anchors can be seen. A video on the real operation of the realized set-up can be found in Reference [19].

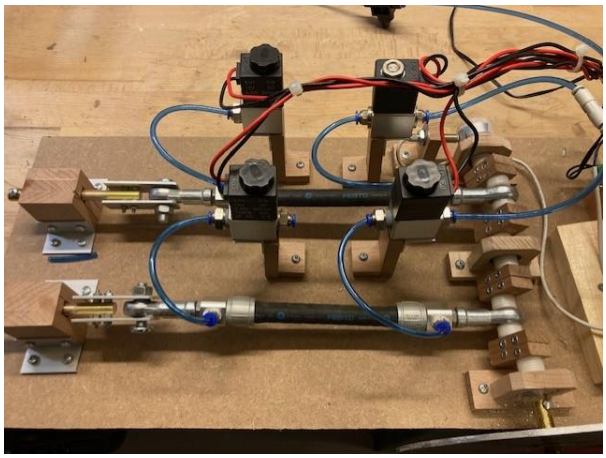

a)

b)

c)

Fig. 11 Top and side view of the compressed air engine a) Side view, b) top view, c) detail of the angular position sensor

6, Control

In figure 12 the complete engine is represented with the artificial muscles a and b coupled to the crankshaft. Each muscle is controlled by an intake valve xin_a (respectively Xin_b) and an exhaust valve xexh_a (respectively xexh_b). The intake valves are opened during the first half-periods of their cycle where the muscles are contracted. They are closed during the return stroke in the second half-period while the corresponding exhaust valves are opened when the muscles go in the relaxing state. The control signals for the valves are generated from a position sensor producing the signal x_control.

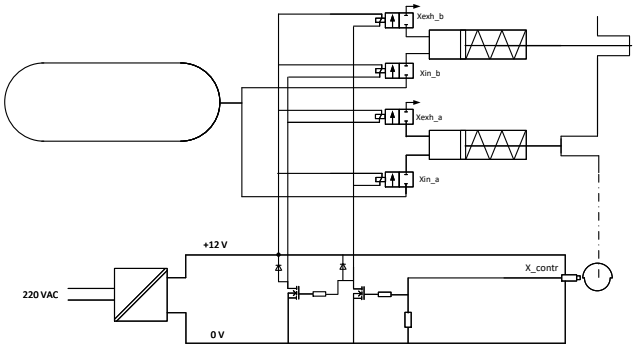

Figure 12 Control of the engine

6.1 Length incompatibility

During the first (respectively the second) half-period of the crankshaft's rotation, the contraction motions of the muscles follow the displacements of the crankpins from the top dead centre (TDC) down to the bottom dead centre (BDC). But

after passing the BDC when the exhaust valves are opened the muscles should be able to recover their original lengths of the relaxed state. These lengths are not compatible with the lengths imposed by the position of the crankpins and would cause a lateral deformation or a bending of the active part of the muscles. Another problem is given by the condition that the length of the active part of the muscle in its contracted state is depending on the pressure of the injected air. These two incompatibilities of lengths can be resolved by adding a device that allows the muscle to elongate during relaxation without producing unwanted torque or movement. This property which is beneficial from the point of view of the lateral deformation of the muscle has a negative consequence on the energy balance, due to the fact that the absorbed deformation energy of the muscle's envelope cannot be transmitted to the crankshaft and must be considered as losses.

A specific device can solve the problem of the pressure-variable contraction motion which can vary independently of the fixed radius of gyration of the crankpin. This device is called the sliding anchor and is described in the following section.

6.2 Sliding anchor

The sliding anchor is mainly composed of a guided rod that allows the anchor point of the active connecting rod to move before and during the upward movement of the crankpin (Figure 13). The bottom position (left position in the figure) of the guided rod is imposed by the effective length of the relaxing muscle, but the upper position (right position in the figure) is limited by a stop where the ring at the end of the rod rests against the guiding tube. The approach to the stop at the top dead center is generally smooth due to the shape of the variation in the effective length as shown in Figure 4 for the corresponding angles (times 0.5 and 1s). Figure 14 shows the realized sliding anchor of the experimental set-up. The upper anchor in the figure corresponds to the active connecting rod of the crankpin which has reached its TDC. Its muscle element goes in contraction after the intake valve is opened, at that time the sliding rod has reached its stop position. The lower anchor in the figure corresponds to the active connecting rod of the crankpin at its BDC. Its muscle element is relaxed after the exhaust valve has opened.

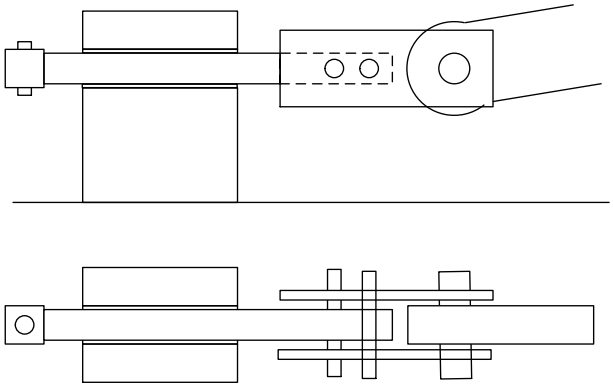

Fig. 13 Side and top view of the sliding anchor.

5. Discussion

The present work was realized with the motivation to establish a basic knowledge on the PAM based engine, which idea was found in Reference 13. The different variables of the system as forces, torque components and mechanical power were simulated.

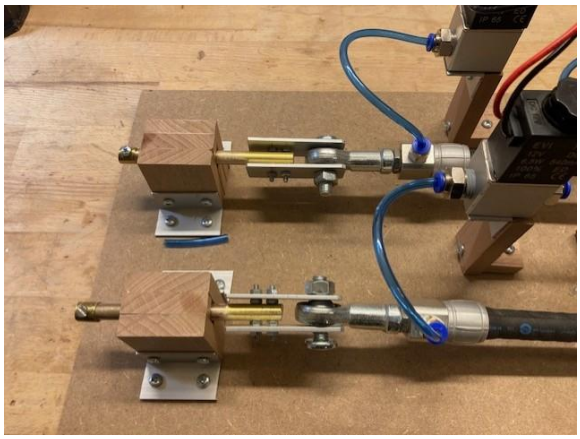

Fig. 14 The realised sliding anchors

Several constraints were discovered (variable contraction length of the PAMs and "invention" of the sliding anchor as a solution. The right operation of the sliding anchor concept was verified experimentally, even if the used materials of the set-up present some small friction. A more elaborated system could be based on linear bearings or use self-lubricating materials. The main result is that the PAM based engine has a poor value of the efficiency, similar to the classical pneumatic actuators and motors in general. This is due to the fact that the compressed air that has filled the active chamber of the actuator is released to the atmosphere after it has produced displacement work. The energetic content of the released air corresponds to the term U of Relation 16. The possibility to increase the efficiency by adding an expansion element as was done for other pneumatic machines (see References 5-7) is not possible due to the nature and way of operation of the artificial muscles.

8. Conclusions

The concept of a compressed air engine based on pneumatic artificial muscles could be verified with the present study where the different variables have been simulated with the help of a kinematic model. The evolution of the contraction forces of the two PAMs coupled to the crankshaft, and the produced torque correspond to the expected behaviour. The relatively strong modulation of the torque has led to the addition of a flywheel element on the shaft of the engine. As supposed at the beginning of the study, the energetic efficiency of the engine only reaches a poor value. The evaluation of the efficiency has been done under ideal conditions where the friction and deformation losses inside the artificial muscles have been neglected. The obtained result however represents a theoretic limit of such a system, and such a result is sufficient to qualify the concept of such an engine as questionable.

9. References

1. Rufer, A., Energy storage-Systems and components, CRC Press, Taylor & Francis group, Boca Raton FL, November, 2017
2. Devang Marvania, Sudhakar Subudhi, A comprehensive review on compressed air powered engine, Renewable and Sustainable Energy Reviews, Volume 70, 2017, Pages 1119-1130, ISSN 1364-0321, https://doi.org/10.1016/j.rser.2016.12.016. (https://www.sciencedirect.com/science/article/pii/S1364032116310681).

3. Atlas Copco, Pocket guide to air motors, 9833 9067 01 2015:1 Jetlag/Boardwalk. Printed in Sweden. © Atlas Copco Industrial Technique AB.
4. Dhumal, A., Ambhore, N., Naik, A. *et al.* Design and Optimization of Air Motor with Gear Rotor System for Enhanced Performance. *J. Inst. Eng. India Ser. C* 106, 367–376 (2025). https://doi.org/10.1007/s40032-024-01157-6.
5. Rufer, A., A High Efficiency Pneumatic Drive System Using Vane-Type Semi-Rotary Actuators, Facta Universitatis, Series: Electronics and Energetics Vol. 34, No 3, September 2021, pp. 415-433, https://doi.org/10.2298/FUEE2103415R.
6. Rufer, A., A High Efficiency Pneumatic Motor Based on Double-Acting Linear Cylinders, World Wide Journal of Multidisciplinary Research and Development, WWJMRD, 2021, 7(1), 25-36.
7. Rufer, A., A four-cylinder pneumatic expansion motor with high efficiency, Academia Green Energy, 2(2), April 2025, DOI: 10.20935/AcadEnergy7625.
8. H. Liu, Y. Chen, G.L. Tao, G.Z. Jia, W.H. Ding, Research on the displacement and stroke-bore ratio of the air-powered engine, Proceedings of the Sixth International Conference on Fluid Power Transmission and Control (2005), pp. 381-384
9. Yidong Fang, Yiji Lu, Anthony Paul Roskilly, Xiaoli Yu, A review of compressed air energy systems in vehicle transport, Energy Strategy Reviews, Volume 33, 2021, 100583, ISSN 2211-467X,
10. Truglia, Vito Gianfranco, High efficiency engine driven by pressurized air or other compressible gases, US Patent, US 9,677.400 B2 Jun. 13, 2017.
11. Nègre, Guy, Engine with an active mono-energy and/or bi-energy chamber with compressed air and/or additional energy and thermodynamic cycle thereof, US Patent, US 7.469,527 B2, Dec. 30, 2008
12. Tong Yi, Chun Jin, Jichao Hong and Yanbo Liu, Layout analysis of compressed air and hydraulic energy storage systems for vehicles, Advances in Mechanical Engineering, 2022, Vol. 14(1) 1–19.
13. Koruku, S., Samtas, G., Soy, G., Design and Experimental Investigation of Pneumatic Movement Mechanism Supported by Mechanic Cam and Crank Shaft, TEM Journal, Volume 4 / Number 1 / 2015, www.temjournal.com.
14. Kanchana Crishan Wickramatunge, Thananchai Leephakpreeda, Study on mechanical behaviors of pneumatic artificial muscle, International Journal of Engineering Science 48 (2010) 188–198, Elsevier.
15. FESTO, Fluidic muscle,
1. https://ftp.festo.com/Public/PNEUMATIC/SOFTWARE_SERVICE/Documentation/2020/DE/DMSP-MAS_DE.PDF.
16. Chivu, C., Static Model and Simulation of a Pneumatic Artificial Muscle, International conference on Economic Engineering and Manufacturing Systems, Brasov, 25-26 October 2007, https://recentonline.ro/021/Chivu_Catalin_01a-R21.pdf.
17. Wafaa Al-Mayahi, Hassanin Al-Fahaam, A Review of Design and Modeling of Pneumatic Artificial Muscle, Iraqi Journal for Electrical and Electronic Engineering, 2024, https://doi.org/10.37917/ijeee.20.1.13.
18. Hao Zheng, Xiangrong Shen, Double-Acting Sleeve Muscle Actuator for Bio-Robotic Systems, *Actuators* 2013, *2*, 129-144; doi:10.3390/act2040129.
19. https://www.youtube.com/watch?v=N1b0VLAVjZg